Cold collisions of heavy $^2\Sigma$ molecules with alkali-metal atoms in a magnetic field: *Ab initio* analysis and prospects for sympathetic cooling of SrOH($^2\Sigma^+$) by Li(^2S)

Masato Morita,[1] Jacek Kłos,[2] Alexei A. Buchachenko,[3,4] and Timur V. Tscherbul[1]
[1]*Department of Physics, University of Nevada, Reno, Nevada 89557, USA*
[2]*Department of Chemistry and Biochemistry, University of Maryland, College Park, Maryland 20742, USA*
[3]*Skolkovo Institute of Science and Technology, Skolkovo Innovation Center, Building 3, Moscow 143026, Russia*
[4]*Department of Chemistry, M. V. Lomonosov Moscow State University, Moscow 119991, Russia*
(Received 15 February 2017; published 26 June 2017)

We use accurate *ab initio* and quantum scattering calculations to explore the prospects for sympathetic cooling of the heavy molecular radical SrOH($^2\Sigma^+$) by ultracold Li atoms in a magnetic trap. Our *ab initio* calculations show that the chemical reaction between spin-polarized Li and SrOH, which occurs on the triplet Li-SrOH potential energy surface (PES), is strongly endothermic and hence energetically forbidden at ultralow temperatures. The chemical reaction Li(^2S) + SrOH($^2\Sigma^+$) → Sr(^1S) + LiOH($^1\Sigma^+$) occurs barrierlessly on the singlet PES and is exothermic by 2505 cm^{-1}. A two-dimensional PES for the triplet electronic state of Li-SrOH is calculated *ab initio* using the partially spin-restricted coupled cluster method with single, double, and perturbative triple excitations and a large correlation-consistent basis set. The highly anisotropic PES has a deep global minimum in the skewed Li-HOSr geometry with $D_e = 4932\,\mathrm{cm}^{-1}$ and saddle points in collinear configurations. Our quantum scattering calculations predict low spin-relaxation rates in fully spin-polarized Li + SrOH collisions with the ratios of elastic to inelastic collision rates well in excess of 100 over a wide range of magnetic fields (1–1000 G) and collision energies (10^{-5} to 0.1 K), suggesting favorable prospects for sympathetic cooling of SrOH molecules with spin-polarized Li atoms in a magnetic trap. We find that spin relaxation in Li + SrOH collisions occurs via a direct mechanism mediated by the magnetic dipole-dipole interaction between the electron spins of Li and SrOH, and that the indirect (spin-rotation) mechanism is strongly suppressed. The upper limit to the Li + SrOH reaction rate coefficient calculated for the singlet PES using adiabatic capture theory is found to decrease from $4\times10^{-10}\,\mathrm{cm}^3/\mathrm{s}$ to a limiting value of $3.5\times10^{-10}\,\mathrm{cm}^3/\mathrm{s}$ with decreasing temperature from 0.1 K to 1 μK.

DOI: 10.1103/PhysRevA.95.063421

I. INTRODUCTION

Ultracold molecular gases offer a wide range of research opportunities, extending from quantum simulation of many-body systems with long-range dipolar interactions [1–3] to external field control of chemical reaction dynamics [2,4,5], precision measurement of molecular energy levels to uncover new physics beyond the standard model [6–9], and quantum information processing with molecular arrays in optical lattices [10]. At present, coherent association of ultracold alkali-metal atoms remains the only experimental technique to produce ultracold gases of polar molecules KRb and NaK [11–13]. Recent advances in laser cooling and magneto-optical trapping [14–18], single-photon cooling [19], Sisyphus laser cooling [20,21], and optoelectrical cooling [21,22] made it possible to control and confine molecular species such as SrF, CaF, SrOH, YO, CH_3F, and H_2CO in electrostatic and magnetic traps at temperatures as low as a fraction of a millikelvin [14–19,21,22]. Due to the intrinsic limitations of optical cooling, it is necessary to employ second-stage cooling techniques to further reduce the temperature of a trapped molecular gas to < 0.1 mK [1,19].

One such technique—sympathetic cooling—relies on elastic atom-molecule collisions to transfer energy and momentum from a cold molecular gas to an ultracold reservoir of neutral atoms. While elastic collisions drive momentum transfer and thermalization, inelastic collisions release the internal energy of the molecules, leading to heating and ultimately trap loss. In order to remain trapped in the inhomogeneous magnetic field of a conservative magnetic trap, open-shell molecules must reside in the low-field-seeking Zeeman states, which contain an excess of internal Zeeman energy. This energy can be released in collisions with buffer-gas atoms in a process known as collision-induced spin relaxation [1,4]. For sympathetic-cooling experiments, it is desirable to keep the molecules in the trap for as long as possible; hence, the rate of collision-induced spin relaxation should be small compared to the elastic collision rate. To allow for efficient thermalization of trapped molecules on the experimental time scale, the ratio of elastic to inelastic collision rates should exceed 100 [1].

Several groups have explored the possibility of using ultracold alkali-metal atoms to sympathetically cool paramagnetic molecules such as OH, NH, CaH, and CaF in a magnetic trap using accurate *ab initio* and quantum scattering calculations. In particular, Lara *et al.* showed that inelastic relaxation in cold Rb + OH collisions occurs at a high rate, thereby precluding sympathetic cooling of magnetically trapped OH by Rb atoms [23]. The spin-relaxation cross sections for collisions of polar radicals NH and OH with spin-polarized N and H atoms were found to be small owing to the weak anisotropy of the high-spin NH-N, NH-H, and OH-H interactions, making atomic nitrogen and hydrogen promising coolant atoms [24–27]. The same conclusion was reached for ground-state Mg atoms colliding with NH($^3\Sigma^-$) molecules [28]. We showed that, despite the strong angular anisotropy of the interactions between $^2\Sigma$ molecular radicals and alkali-metal atoms, the inelastic cross sections for interspecies collisions are strongly suppressed due to the weakness of the spin-rotation interaction in $^2\Sigma$ molecules [29]. Small polyatomic molecular radicals such as

methylene (CH_2), methyl (CH_3), and amidogen (NH_2) were found to have small spin-relaxation cross sections with S-state atoms, and hence were suggested as promising candidates for sympathetic-cooling experiments in a magnetic trap [30,31]. Magnetic trapping of CH_3 radicals was accomplished in a recent experiment [32].

The vast majority of atom-molecule combinations proposed for sympathetic-cooling experiments included light hydrogen-containing molecules such as NH, OH, and CaH. These molecules have large rotational level spacings and low densities of rovibrational states, facilitating accurate quantum scattering calculations [29,33]. In contrast, the heavy molecular radicals produced and studied in recent experiments (CaF, SrF, YO, and SrOH) have small rotational constants and dense spectra of rovibrational states. While the possibility of co-trapping and sympathetic cooling of $^2\Sigma$ molecular radicals with ultracold alkali-metal atoms has been suggested [19,20,29], numerically exact quantum scattering calculations of their collisional properties are challenging [29] due to the strongly anisotropic atom-molecule interactions, which couple a large number of rovibrational states and field-induced mixing between different total angular momenta (see Ref. [34] for a detailed discussion). As a result, it remains unclear whether heavy molecular radicals trapped in recent experiments [14–19] have small enough inelastic collision rates with ultracold alkali-metal atoms to allow for efficient sympathetic cooling in a magnetic trap.

Cooling and trapping polyatomic molecular radicals is expected to provide new insights into many-mode vibrational dynamics, photochemistry, and chemical reactivity at ultralow temperatures [20,30–32,35–37]. Recently, Kozyryev *et al.* used buffer-gas cooling to prepare a cold sample of the strontium monohydroxide radical [SrOH ($X^2\Sigma^+$)] in the ground and first excited vibrational states and to observe vibrational energy transfer between the states induced by collisions with He atoms at 2 K [35]. The highly diagonal array of Franck-Condon factors between the ground $\tilde{X}^2\Sigma^+$ and the first excited $\tilde{A}\Pi_{1/2}$ electronic states of SrOH enables efficient photon cycling, making SrOH an attractive candidate for molecular laser cooling and trapping. In a series of recent experiments, Kozyryev *et al.* observed the radiation pressure force and demonstrated Sisyphus laser cooling of SrOH to below 1 mK in one dimension [20,36].

Here, we use accurate *ab initio* and quantum scattering calculations to explore the possibility of sympathetic cooling of SrOH($^2\Sigma^+$) with ultracold Li(^2S) atoms in a magnetic trap. To this end, we develop an *ab initio* potential energy surface (PES) for the triplet electronic state of Li-SrOH (Secs. II A–II C) and employ it in multichannel quantum scattering calculations using a computationally efficient total angular momentum representation for molecular collisions in magnetic fields [38] (Sec. II D). In Sec. III A we show that inelastic spin relaxation of spin-polarized SrOH molecules in collisions with spin-polarized Li atoms occurs 100 to 1000 times slower than elastic collisions over a wide range of collision energies and magnetic fields, suggesting good prospects of sympathetic cooling of SrOH molecules with ultracold Li atoms in a magnetic trap. We find broad resonance features in the magnetic field dependence of atom-molecule scattering cross sections and show that spin relaxation in cold Li + SrOH collisions occurs predominantly due to the magnetic dipole-dipole interaction (direct mechanism) rather than via the intramolecular spin-rotation interaction combined with the anisotropy of the interaction potential (indirect mechanism). In Sec. III C we use adiabatic capture theory to estimate the upper limit to the rate of the Li + SrOH → LiOH + Sr chemical reaction. The paper concludes in Sec. IV with a summary of main results and a brief outline of future research directions. Atomic units are used throughout the rest of the paper unless otherwise stated.

II. THEORY AND COMPUTATIONAL METHODOLOGY

A. *Ab initio* calculations

The SrOH radical is a linear molecule in its ground electronic state of $^2\Sigma^+$ symmetry [39]. The interaction with a ground-state Li(^2S) atom gives rise to two adiabatic PESs of singlet and triplet spin multiplicities, as shown schematically in Fig. 1. The triplet-singlet couplings have been shown to be negligible in a closely related Li-CaH system [40] and since our interest here is in collisions of fully spin-polarized Li and SrOH which occur on the triplet PES, we make the common assumption of neglecting the difference between the singlet and triplet PESs [24–27,29]. This has the added advantage that single-reference electronic structure methods can be used to describe the triplet state of the Li-SrOH collision complex. To compute the triplet PES, we thus employ the partially spin-restricted coupled cluster method [41] with single, double, and perturbative triple excitations [RCCSD(T)] with the reference wave function taken from the restricted Hartree-Fock (RHF) approach. The RHF wave function was calculated using pseudocanonical orbitals from multiconfiguration self-consistent field [42,43] (MCSCF) calculations with valence active space as a starting point.

The geometry of the complex is described by the Jacobi coordinates R, the distance between Li and the center of mass of SrOH; r, the SrOH bond length; and θ, the angle between the Jacobi vectors $\boldsymbol{R}$ and $\boldsymbol{r}$. The origin of the coordinate system is taken at the center of mass of SrOH. The geometry of SrOH is kept linear and fixed throughout the calculations. The position of the center of mass was calculated using the exact mass of the most abundant isotope, ^{88}Sr. The Jacobi angle θ describes the angular dependence of the PES and the $\theta = 0^\circ$ geometry describes the Li–H-O-Sr collinear arrangement. The linear Sr-O-H geometry is described by the bond lengths $r(\mathrm{SrO}) = 2.1110$ Å and $r(\mathrm{OH}) = 0.9225$ Å as verified by the geometry optimization at the RCCSD(T) level. The normal modes of SrOH are determined from the vibrational frequency RCCSD(T) calculations with the same basis set as the PES calculations (excluding the bond functions), which show the doubly degenerate SrOH bending mode at 386 cm^{-1}, the Sr-O stretching mode at 534 cm^{-1}, and the OH stretching vibration at 3919 cm^{-1}.

For the Sr atom, we use a pseudopotential-based augmented correlation-consistent quintuple-zeta basis (aug-cc-pV5Z-PP) of Peterson and co-workers [44] with Stuttgart-Cologne effective core potential (ECP) (ECP28MDF) [45]. The remaining Li, O, and H atoms are described by Dunning's core-valence aug-cc-pCVTZ basis functions [46]. The basis set used in the calculations of the Li-SrOH complex is augmented with a set of $3s3p2d2f1g$ bond functions placed on an ellipsoid as shown

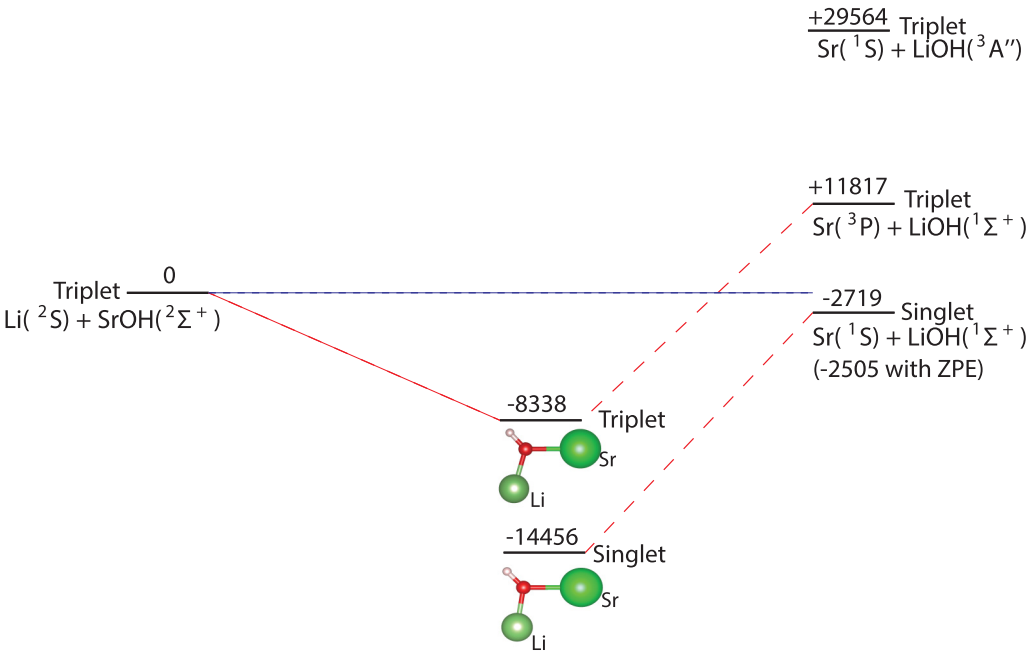

FIG. 1. Correlation diagram for the Li + SrOH → Sr + LiOH chemical reaction. The level energies are expressed in units of cm^{-1}. All the structures have been optimized with the RCCSD(T) method as described in the text except that no bond functions were used and the BSSE correction was not applied.

in the inset of Fig. 2 [47]. The bond functions were represented using the following exponents: $sp = (0.94,0.34,0.12)$, $df = (0.64,0.23)$, and $g = (0.35)$. The ellipsoidal placement of the midbond functions avoids accidental overlap with the atomic basis functions of SrOH at small R.

B. Li-SrOH reaction pathways

To characterize the stationary points along the $Li(^2S) + SrOH(^2\Sigma^+) \rightarrow LiOH + Sr$ reaction paths, we carried out RCCSD(T) calculations using the same methodology as described above. The correlation diagram for the Li + SrOH → LiOH + Sr reaction is shown in Fig. 1. The global minimum of the $S = 1$ (triplet) PES describing the interaction of spin-polarized reactants corresponds to a strongly bound Li-SrOH complex with a binding energy of 8338 cm^{-1} relative to the Li + SrOH asymptote. The $S = 0$ (singlet) PES is bound by 14 456 cm^{-1}. These binding energies are qualitatively similar to those reported earlier for similar molecules such as Me_2OH (with Me = Li, Na, or K) [48], which range from 12066.5 to 7939.4 cm^{-1}.

The equilibrium geometry parameters of LiOH and SrOH optimized in this work are given in Table I along with the molecular vibrational frequencies, zero-point energies (ZPE) and binding energies. The lowest electronically excited triplet state is found to correspond to a bent LiOH structure with the wave function belonging to the $^3A''$ symmetry. Note that the ground-state binding energy of LiOH is significantly larger than that of SrOH.

The optimized geometries of the triplet and singlet Li-SrOH reaction complexes are shown in Fig. 1. The planar equilibrium structure of the triplet electronic state is bent, characterized by the bond distances $r_{SrO} = 2.27406$ Å, $r_{LiO} = 1.79474$ Å, and $r_{OH} = 0.9604$ Å and bond angles $\angle SrOH = 131.8^\circ$ and $\angle SrOLi = 106.2^\circ$. We find that the minimum-energy path from the Li + SrOH collision pair to the triplet Li-SrOH complex is barrierless. The optimized geometry of the singlet Li-SrOH complex is similar to that of the triplet complex, with $r_{SrO} = 2.30470$ Å, $r_{LiO} = 1.75546$ Å, $r_{OH} = 0.96113$ Å, $\angle SrOH = 133.0^\circ$, and $\angle SrOLi = 98.5^\circ$.

Assuming that the total spin S of the Li-SrOH complex is conserved during the chemical reaction [40,49,50], the Li + SrOH reactants evolving on the singlet PES can only form singlet $Sr(^1S)$ + $LiOH(^1\Sigma^+)$ reaction products. Our RCCSD(T) calculations show that the $Li(^2S)+SrOH(^2\Sigma^+)\rightarrow$

TABLE I. Optimized geometry parameters and vibrational frequencies of the reactant and product molecules XOH, where X = Li, Sr. Interatomic distances and angles are given in angstroms and degrees, respectively. Vibrational frequencies, zero-point energies (ZPEs), and binding energies D_e are given in cm^{-1}. The binding energies are calculated with respect to the $X + OH(^2\Pi)$ dissociation limit. ν(OH) denotes the vibrational frequency of the OH stretch, ν_b denotes the MeOH bending frequency, and $\nu(XO)$ the XO bond-stretching frequency.

MeOH	$r(XO)$	r(OH)	$\angle XOH$	ν(OH)	ν_b	$\nu(XO)$	ZPE	D_e
$LiOH(^1\Sigma^+)$	1.586	0.9511	180	3996.5	358.6	942.8	2828.2	69 285
$LiOH(^3A'')$	2.023	0.9810	110	3580.6	366.6	345.1	2146.1	35 326
$SrOH(^2\Sigma^+)$	2.111	0.9220	180	3918.6	387.7	534.2	2614.1	49 031

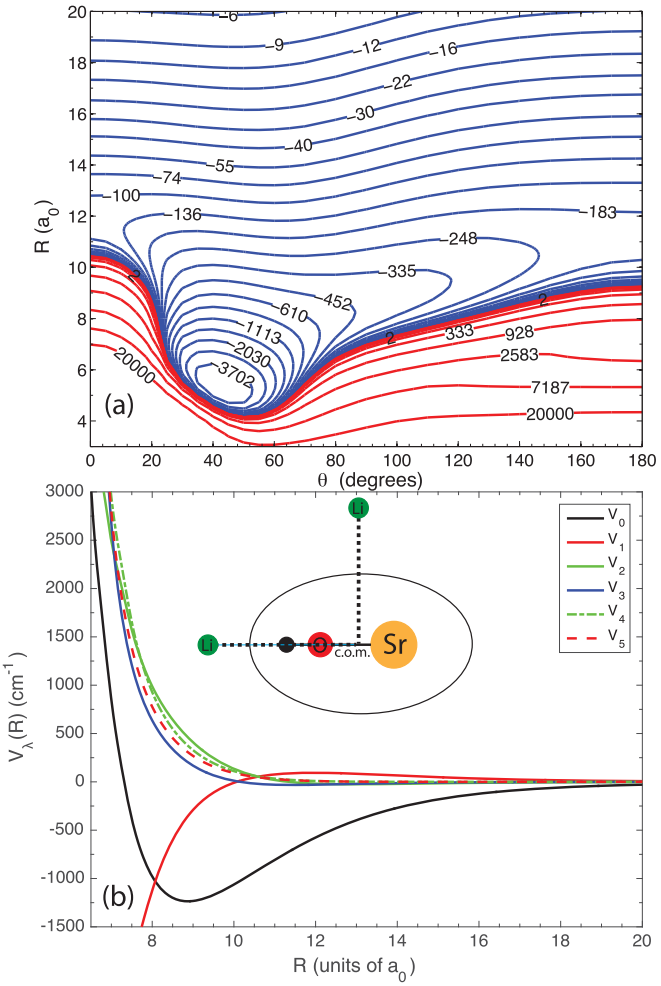

FIG. 2. (a) A contour plot of the *ab initio* potential energy surface for Li-SrOH in its triplet electronic state (in units of cm^{-1}). The $\theta = 0^\circ$ geometry corresponds to the collinear Li–H-O-Sr arrangement. (b) The radial dependence of the first few Legendre expansion coefficients $V_\lambda(R)$. The inset shows the ellipsoid along which the bond functions are placed. The center of the ellipsoid is located at the center of mass of SrOH, and its horizontal and vertical axes are given by $r_b = R_{\text{Li-H}}/2 + r_{\text{H-}X}$ and $r_a = R/2$, where $r_{\text{H-}X}$ is the distance from H to the center of mass of SrOH.

$Sr(^1S)$+LiOH($^1\Sigma^+$) reaction is exothermic by 2505 cm^{-1} including ZPE correction, which agrees well with the value 2581 cm^{-1} calculated using thermochemical data [51]. The calculations predict that the ^3P excited state of Sr lies 14 535 cm^{-1} above the ^1S ground state, again in good agreement with the spectroscopically derived value of 14 703 cm^{-1} [52]. The Li + SrOH reaction evolving on the triplet PES correlates with the $Sr(^3P)$ + LiOH($^1\Sigma^+$) product limit, which is endothermic by 11 817 cm^{-1} (without ZPE correction) as shown in Fig. 1. The other triplet product channel [$Sr(^1S)$ + LiOH($^3A''$)] is even more endothermic. We conclude that while the singlet reaction pathway is energetically allowed and strongly exothermic, both of the triplet pathways are energetically forbidden at low temperatures. Thus, in the absence of *S*-changing mechanisms, the chemical reaction Li + SrOH → Sr + LiOH will not occur on the triplet PES. We note that the *S*-changing mechanisms can be mediated by nonadiabatic interactions [40], long-range magnetic dipole-dipole interactions, and intramolecular spin-rotation couplings [49,50], all of which are expected to be weak in light atom-molecule collision complexes.

C. Triplet Li-SrOH PES in the entrance reaction channel

We calculate the two-dimensional (2D) triplet Li-SrOH PES on a grid of R and θ within a supermolecular approach and correct for the basis-set superposition error (BSSE) using the counterpoise correction procedure of Boys and Bernardi [53]:

$$V(R,\theta) = E_{\text{Li-SrOH}}(R,\theta) - E_{\text{Li-ghost}}(R,\theta) - E_{\text{SrOH-ghost}}(R,\theta). \quad (1)$$

The "ghost" in the above equation denotes the presence of dimer-centered basis functions during the calculations of monomer energies. The R Jacobi coordinate is represented by the radial grid of 105 points spanning distances from $R = 2.75a_0$ to $R = 40a_0$ with a variable step from $0.05a_0$ in the medium range to $0.5a_0$−$2.0a_0$ in the long range. The angular variable θ is represented on a grid of 26 points, with a step of 5° from 0° to 70° and with the step of 10° in the remaining interval to 180°. This gives around 2700 points representing the triplet Li-SrOH PES for a fixed SrOH equilibrium geometry. All electronic structure calculations have been performed with the MOLPRO suite of programs [54,55].

The calculated PES data points are expanded in Legendre polynomials:

$$V(R,\theta) = \sum_{\lambda=0}^{20} V_\lambda(R) P_\lambda(\cos\theta). \quad (2)$$

Figure 2(a) shows a contour plot of the triplet Li-SrOH PES. The potential is extremely anisotropic, varying from strongly attractive (thousands of cm^{-1}) in the region of the global minimum to weakly attractive (−100 to 200 cm^{-1}) near the collinear saddle points at $\theta = 0^\circ$ or $\theta = 180^\circ$ and $R \approx 12a_0$. The high anisotropy is also manifested in the large magnitude of the first few anisotropic Legendre moments $V_\lambda(R)$ shown in Fig. 2(b) at medium and short R. Higher-order Legendre terms become progressively less important at larger atom-molecule separations. The long-range fit is performed using the analytical formula $V_{\text{LR}}(R,\theta) = -\sum_{n,l} \frac{C_{nl}}{R^n} P_l(\cos\theta)$ including the dispersion coefficients from C_{60} to C_{84}. The isotropic van der Waals dispersion coefficient of the triplet PES is estimated from the long-range fit to be $C_{60} = 1.7\times10^9$ $cm^{-1}a_0^6$. The long-range fit is smoothly joined with the expansion fit [Eq. (2)] by the hyperbolic tangent switching function. The radial V_λ coefficients are fit using the reproducing kernel Hilbert space (RKHS) interpolation method with a one-dimensional radial kernel with $n = 2$ and $m = 5$ [56,57]. A FORTRAN routine for the Li-SrOH PES is available in the Supplemental Material [58].

The minimum of the 2D triplet Li-SrOH PES is located at $R_e = 5.289a_0$ and $\theta_e = 43.19^\circ$ with a well depth of 4931.94 cm^{-1}. As shown in Fig. 1, the global minimum of the triplet Li-SrOH complex corresponds to a skewed Li-HOSr geometry with the Li-H distance of $3.818a_0$ and the SrOH-Li angle of ≈71.5°.

D. Quantum scattering calculations

In order to solve the quantum scattering problem for Li-SrOH, we numerically integrate the close-coupling (CC) equations in the body-fixed (BF) coordinate frame [29,38]. Motivated by the need to reduce the computational cost of quantum scattering calculations, we assume that SrOH remains frozen at its ground-state equilibrium configuration, thereby invoking the rigid-rotor approximation [29]. The energy gap between the ground and the lowest excited vibrational states of SrOH (386 cm^{-1}) is small compared to the Li-SrOH potential strength (4931.9 cm^{-1}), which may lead to a temporary excitation of the vibrational modes, giving rise to a resonance structure in the energy and field dependence of scattering cross sections. At collision energies far detuned from the resonances, the coupling between the different vibrational modes of SrOH induced by the interaction with the incident Li atom is small and the rigid-rotor approximation is expected to hold. We therefore expect that our calculations provide a reasonably accurate description of cold Li + SrOH background scattering.

The effective Hamiltonian for low-energy collisions between an atom A (^2S) and a diatomic molecule B ($^2\Sigma$) in the presence of an external magnetic field may be written [29,38]

$$\hat{\mathcal{H}} = -\frac{1}{2\mu}R^{-1}\frac{\partial^2}{\partial R^2}R + \frac{(\hat{J}-\hat{N}-\hat{S}_A-\hat{S}_B)^2}{2\mu R^2} + \hat{\mathcal{H}}_A + \hat{\mathcal{H}}_B + \hat{\mathcal{H}}_{\rm int}, \quad (3)$$

where μ is the reduced mass of collision complex defined by $\mu = m_A m_B/(m_A+m_B)$, $\hat{\mathcal{H}}_A$ and $\hat{\mathcal{H}}_B$ describe separated A and B in an external magnetic field, and $\hat{\mathcal{H}}_{\rm int}$ describes the interaction between the collision partners. As mentioned in Sec. II A the collision complex is described by the Jacobi vectors $\boldsymbol{R}$ and $\boldsymbol{r}$ in the BF frame. The embedding of the BF z axis is chosen to coincide with the vector $\boldsymbol{R}$, and the BF y axis is chosen to be perpendicular to the plane defined by the collision complex.

In Eq. (3), $\hat{J}$ is the operator for the total angular momentum of the collision complex, $\hat{N}$ is the rotational angular momentum operator for molecule B, and $\hat{S}_A$ and $\hat{S}_B$ are the spin operators for atom A and molecule B, respectively. The orbital-angular-momentum operator of the collision complex in the BF frame is given by $\hat{l} = \hat{J}-\hat{N}-\hat{S}_A-\hat{S}_B$. The separated atom Hamiltonian in the presence of an external magnetic field is given as $\hat{\mathcal{H}}_A = g_e\mu_B\hat{S}_{A,Z}B$, where g_e is the electron g-factor, μ_B is the Bohr magneton, $\hat{S}_{A,Z}$ gives the projection of $\hat{S}_A$ onto the magnetic field axis, and B is the magnitude of the external magnetic field. For a linear molecule such as SrOH($X^2\Sigma^+$), $\hat{\mathcal{H}}_B = B_e\hat{N}^2 + \gamma_{\rm SR}\hat{N}\cdot\hat{S}_B + g_e\mu_B\hat{S}_{B,Z}B$, where B_e is the rotational constant, and $\gamma_{\rm SR}$ is the spin-rotation constant. The last term in Eq. (3) describes the atom-molecule interaction, including both the electrostatic interaction potential $\hat{V}$ and the magnetic dipole-dipole interaction $\hat{V}_{\rm dd}$ between the magnetic moments of the atom and the molecule. The interaction potential $\hat{V}$ may be written

$$\hat{V}(R,\theta) = \sum_{S=|S_A-S_B|}^{S_A+S_B}\sum_{\Sigma=-S}^{S}|S\Sigma\rangle\hat{V}^S(R,\theta)\langle S\Sigma|, \quad (4)$$

where total electronic spin S is defined as $\hat{S} = \hat{S}_A + \hat{S}_B$. Our interest here is in collisions between rotationally ground-state SrOH molecules ($N=0$) with Li atoms initially in their maximally stretched Zeeman states $M_{S_A} = M_{S_B} = 1/2$, where M_{S_A} and M_{S_B} are the projections of $\hat{S}_A$ and $\hat{S}_B$ onto the space-fixed (SF) Z axis. Following our previous work on Li-CaH [29,40] we assume that the nonadiabatic coupling between the triplet ($S=1$) and the singlet ($S=0$) Li-SrOH PESs can be neglected, and that the PESs are identical, i.e., $\hat{V}^{S=0}(R,\theta) = \hat{V}^{S=1}(R,\theta)$. The dipolar interaction between the magnetic moments of the atom and molecule may be written [33]

$$\hat{V}_{\rm dd} = -g_e^2\mu_0^2\sqrt{\frac{24\pi}{5}}\frac{\alpha^2}{R^3}\sum_q(-)^q Y^*_{2,-q}(\hat{\boldsymbol{R}})[\hat{S}_A\otimes\hat{S}_B]^{(2)}_q, \quad (5)$$

where μ_0 is the magnetic permeability of free space, α is the fine-structure constant, and $[\hat{S}_A\otimes\hat{S}_B]^{(2)}_q$ is the spherical tensor product of $\hat{S}_A$ and $\hat{S}_B$.

Following previous studies [29,33,38], the total wave function of the Li-SrOH collision complex is expanded in a set of basis functions

$$|JM\Omega\rangle|NK_N\rangle|S_A\Sigma_A\rangle|S_B\Sigma_B\rangle. \quad (6)$$

Here, Ω, K_N, Σ_A, and Σ_B are the projections of J, N, S_A, and S_B onto the BF quantization axis z, and $\Omega = K_N+\Sigma_A+\Sigma_B$ is satisfied. Unlike Ω, the projection of J onto the SF quantization axis M is rigorously conserved for collisions in a dc magnetic field [1,59], so the CC equations can be constructed and solved independently for each value of M. In Eq. (6) $|JM\Omega\rangle = \sqrt{(2J+1)/8\pi^2}D^{J*}_{M\Omega}(\bar{\alpha},\bar{\beta},\bar{\gamma})$ is an eigenfunction of the symmetric top, and the Wigner D functions $D^{J*}_{M\Omega}(\bar{\alpha},\bar{\beta},\bar{\gamma})$ depend on the Euler angles $\bar{\alpha}$, $\bar{\beta}$, and $\bar{\gamma}$, which specify the position of the BF axes x, y, and z in the SF frame. The rotational degrees of freedom of SrOH in the BF frame are described by the functions $|NK_N\rangle$, which can be expressed in terms of the spherical harmonics as $\sqrt{2\pi}Y_{NK_N}(\theta,0)$. The matrix elements of the effective Hamiltonian in the total angular momentum basis (6) are evaluated as described elsewhere [38].

The molecular parameters used in scattering calculations are listed in Table II. The size of the basis set is governed by the truncation parameters of $J_{\rm max}$ and $N_{\rm max}$ which are the maximum values of J and N in the basis set. Unless stated otherwise, all scattering calculations are carried out with $J_{\rm max}=3$. The convergence properties with respect to $J_{\rm max}$ are examined in the Appendix. Due to the strong anisotropy of the Li-SrOH interaction, a large number of rotational channels

TABLE II. Spectroscopic constants of SrOH (in cm^{-1}) and masses of the collision partners (in amu) used in scattering calculations.

Parameter	Value
B_e	0.24633
$\gamma_{\rm SR}$	2.4275×10^{-3}
$m_{\rm SrOH}$	104.9083586
$m_{\rm Li}$	7.01600455

must be included in the basis set to obtain converged results. Furthermore, the rotational constant of SrOH is ∼20 times smaller than that of CaH, which results in larger values of $N_{\max}$ for Li-SrOH compared to Li-CaH ($N_{\max} = 55$ [29]). Indeed, we found that using $N_{\max} = 115$ is necessary to obtain the cross sections converged to within 2% (see the Appendix).

The numerical procedures used in this work are essentially the same as those employed in our previous study of Li-CaH collisions [29] as explained in detail elsewhere [33,38]. In brief, the CC equations are solved numerically using the log-derivative propagator method [60,61] on an equidistant radial grid from $R_{\min} = 4.0a_0$ to R_{mid} with $R_{\mathrm{mid}} = 9.5a_0$ for $B > 10$ G and $R_{\mathrm{mid}} = 22.7a_0$ for $B \leqslant 10$ G using a step size of $0.00189a_0$. Airy propagation is employed for $R_{\mathrm{mid}} \leqslant R \leqslant R_{\max}$ with $R_{\max} = 280.0a_0$ for $B > 10$ G and $R_{\max} = 1322.8a_0$ for $B \leqslant 10$ G. Propagating the log-derivative matrix out to very large values of $R_{\max}$ is necessary to maintain the numerical accuracy of quantum scattering calculations on systems with long-range anisotropic interactions at low magnetic fields [62].

After propagating the log-derivative matrix out to a sufficiently large $R = R_{\max}$ where the interaction potential becomes negligible, the matrix is transformed from the total-angular-momentum representation to a basis set in which $\hat{\mathcal{H}}_A$, $\hat{\mathcal{H}}_B$, and $\hat{l}^2$ are diagonal. The resultant log-derivative matrix is matched to the scattering boundary conditions to obtain the S matrix, and the elastic and inelastic cross sections are extracted from the S matrix as described in Ref. [38].

E. Quantum capture calculations

As argued in Sec. II B, the chemical reaction of spin-polarized reactants is energetically forbidden at low collision energies. However, spin-nonconserving interactions, which are not accounted for within our 2D single-state model, may induce nonadiabatic transitions to the singlet PES [40]. An upper bound to the rate of these transitions is given by the capture rate, i.e., the rate of reactant penetration to the short-range region as defined classically by the Langevin model. To estimate this rate, we applied here a quantum version of the statistical adiabatic channel model [63] implemented as described in Ref. [64].

In brief, we use a simplified atom-molecule Hamiltonian (3) without the spin-rotation coupling and Zeeman interactions. The adiabatic channel potentials are obtained by diagonalizing the Hamiltonian, at fixed atom-molecule separations R, in the symmetry-adapted rigid-rotor eigenfunction basis set. Since we are only interested in the channels correlating to the ground rotational state of the SrOH reactant, the single lowest-energy root was retained for each total-angular-momentum quantum number J ($l \equiv J$ in this case). Using $N_{\max} = 49$ gives results converged to within 2% for the desirable $N = 0$ adiabatic channel near the bottom of the potential well at $R = 5.3a_0$.

To calculate the quantum capture probabilities for $J \leqslant 20$, we use the modified Truhlar-Kupperman finite difference method [65] as described in Refs. [63,64] on a grid of collision energies extending from 10^{-11} to 1000 cm^{-1}. Inner capture boundary conditions are applied at $R = R_0$ within the short-range region. We used six values of $R_0 \in [5.7, 13.2]a_0$ to obtain the average capture probability at each collision energy.

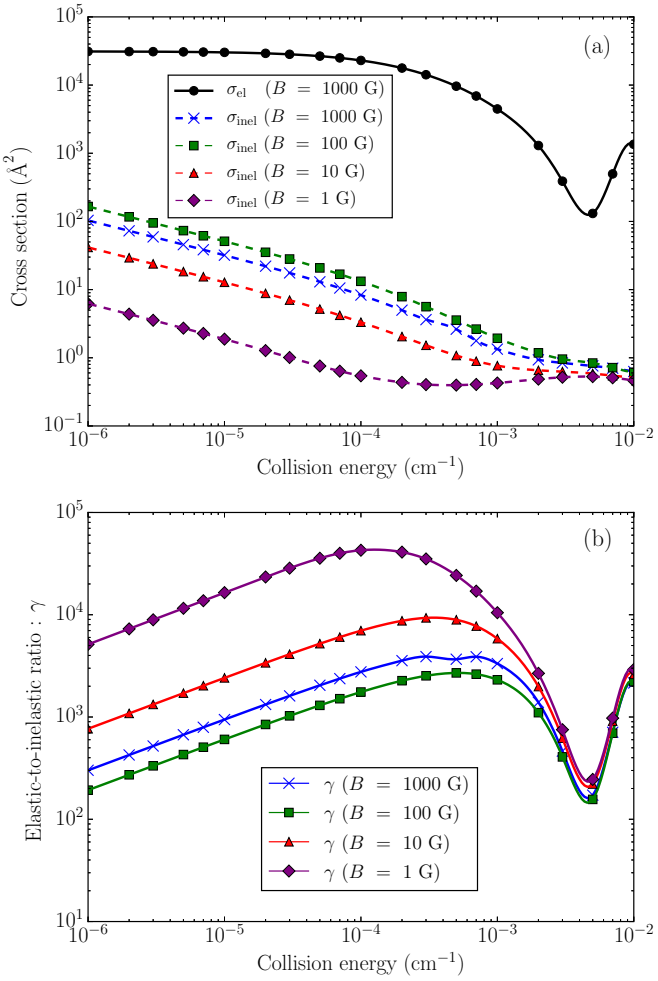

FIG. 3. (a) Cross sections for elastic scattering and inelastic spin relaxation in spin-polarized Li + SrOH collisions plotted as functions of collision energy for the external magnetic fields of 1 G (diamonds), 10 G (triangles), 100 G (squares), and 1000 G (crosses). The elastic cross section displays a very weak magnetic field dependence. (b) The ratios of elastic and inelastic cross sections as functions of collision energy for the same values of the magnetic field as in (a).

The classical capture probabilities are determined from the height of the centrifugal barrier for each $J \leqslant 40$ [64].

III. RESULTS

A. Elastic and inelastic cross sections

Figure 3(a) shows the elastic (σ_{el}) and inelastic (σ_{inel}) cross sections for fully spin-polarized Li + SrOH collisions as functions of collision energy for the external magnetic fields of 1, 10, 100, and 1000 G. Due to the very weak magnetic field dependence of the elastic cross section, only the $B = 1000$ G result is shown in the figure. The inelastic cross section increases significantly as the magnetic field increases from 1 to 100 G, especially in the ultracold s-wave regime (the field dependence is explored later in this section). The inelastic cross sections as a function of collision energy remain smooth and small over the entire energy range considered. As mentioned in the Introduction, for sympathetic cooling to be effective, the

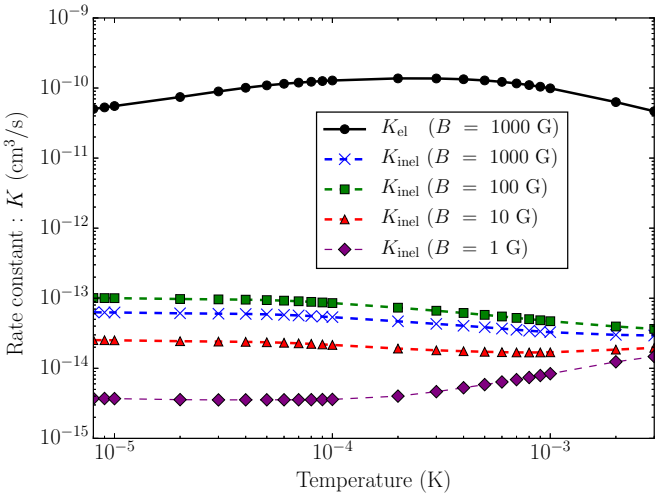

FIG. 4. Temperature dependence of the rate constants for elastic scattering (circles) and inelastic spin relaxation in spin-polarized Li + SrOH collisions calculated for the magnetic field values of 1 G (diamonds), 10 G (triangles), 100 G (squares), and 1000 G (crosses).

ratio of elastic to inelastic cross sections, $\gamma = \sigma_{el}/\sigma_{inel}$, must exceed 100. Figure 3(b) shows that the calculated values of γ do exceed 100 throughout the whole energy range except in the vicinity of $E_C = 5.0\times10^{-3}\,\mathrm{cm}^{-1}$.

Figure 4 shows the temperature dependence of the rate constants for elastic scattering and spin relaxation. The rate constant is an energy-averaged property obtained by the convolution of the cross sections with the Maxwell-Boltzmann distribution function. As such, the behavior of the rate constant as a function of temperature tends to be monotonous. Importantly, the rate of collision-induced spin relaxation is more than two orders of magnitude smaller than that of elastic scattering, suggesting favorable prospects for sympathetic cooling of SrOH molecules with Li atoms in a magnetic trap.

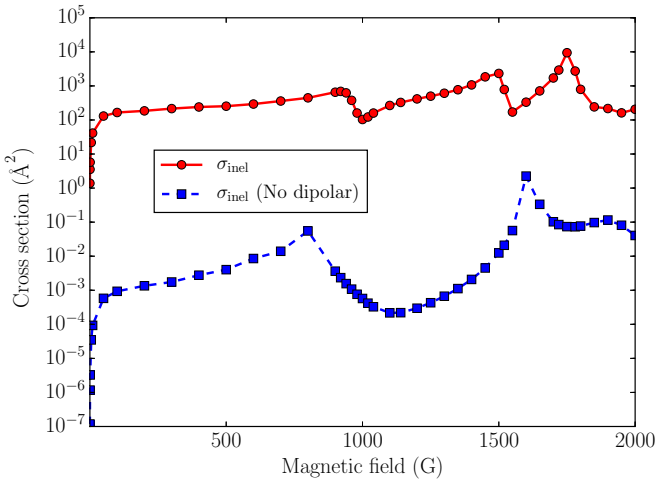

FIG. 5. Magnetic field dependence of the inelastic cross sections for Li + SrOH calculated with (solid line with circles) and without (dashed line with squares) the magnetic dipole-dipole interaction. The collision energy is $1.0\times10^{-6}\,\mathrm{cm}^{-1}$.

In Fig. 5, we plot the magnetic field dependence of the inelastic cross sections calculated for the collision energy of $1\times10^{-6}\,\mathrm{cm}^{-1}$. We observe two broad asymmetric resonance profiles, around which the inelastic cross sections are reduced dramatically. This suggests the possibility of suppressing spin relaxation in Li + SrOH collisions by tuning the dc magnetic field as noted previously for He-O_2 [66]. We note that, despite the high density of rovibrational states of the Li-SrOH collision complex, only a few resonances are observed in the inelastic cross section below 2000 G. This suggests that most of the states of the complex are decoupled from the incident spin-polarized collision channel. A similar magnetic field dependence is observed in ultracold collisions of spin-polarized alkali-metal atoms [67,68] and $O_2(^3\Sigma)$ molecules [69,70], which display a lower resonance density in non-spin-polarized initial channels.

B. Direct versus indirect spin-relaxation mechanisms

In general, inelastic spin relaxation in cold collisions of $^2\Sigma$ molecules in their ground rotational states with ^2S atoms is mediated by two mechanisms, direct and indirect [29,71]. The direct mechanism is due to the long-range intermolecular magnetic dipole-dipole interaction $\hat{V}_{dd}$ given by Eq. (5) [29,62]. The indirect mechanism is due to a combined effect of the intramolecular spin-rotation interaction and the coupling between the rotational states of the molecule induced by the anisotropy of the interaction potential [71]. As shown in Fig. 2(a), the anisotropy of the interaction potential is strong in the range of small atom-molecule distances R; thus the indirect mechanism operates at short range.

In order to compare these mechanisms, we plot in Fig. 5 the magnetic field dependence of the inelastic cross sections calculated with and without the magnetic dipole-dipole interaction. Omitting the magnetic dipole-dipole interaction leads to a dramatic reduction of the inelastic cross section over the entire magnetic field range (including near scattering resonances), which strongly suggests that spin relaxation in spin-polarized Li + SrOH collisions is driven by the direct mechanism. As shown in Fig. 6(a), the indirect mechanism becomes more efficient with increasing collision energy; however, the direct mechanism dominates even at the highest collision energy considered.

It is instructive to compare the efficiency of the indirect spin-relaxation mechanism in collisions of light (CaH) and heavy (SrOH) molecular radicals with Li atoms. The inelastic cross sections calculated in the absence of the magnetic dipole-dipole interaction are similar in magnitude (5.7×10^{-4} Å for Li + SrOH and 10^{-3} Å for Li + CaH [29] at $E_C = 1\times10^{-6}\,\mathrm{cm}^{-1}$ and $B = 1000$ G). At first glance, this is surprising because ~120 excited rotational states contribute to the indirect spin-relaxation mechanism for Li + SrOH, as opposed to only ~50 rotational states for Li + CaH. As a result, the number of third- and higher-order contributions to the Li + SrOH inelastic scattering amplitude is expected to be significantly larger than for Li + CaH, leading one to expect the indirect spin-relaxation mechanism to be more efficient for Li + SrOH. However, the spin-rotation constant of SrOH is ten times smaller than that of CaH, so each contribution to the Li + SrOH scattering amplitude is suppressed by a

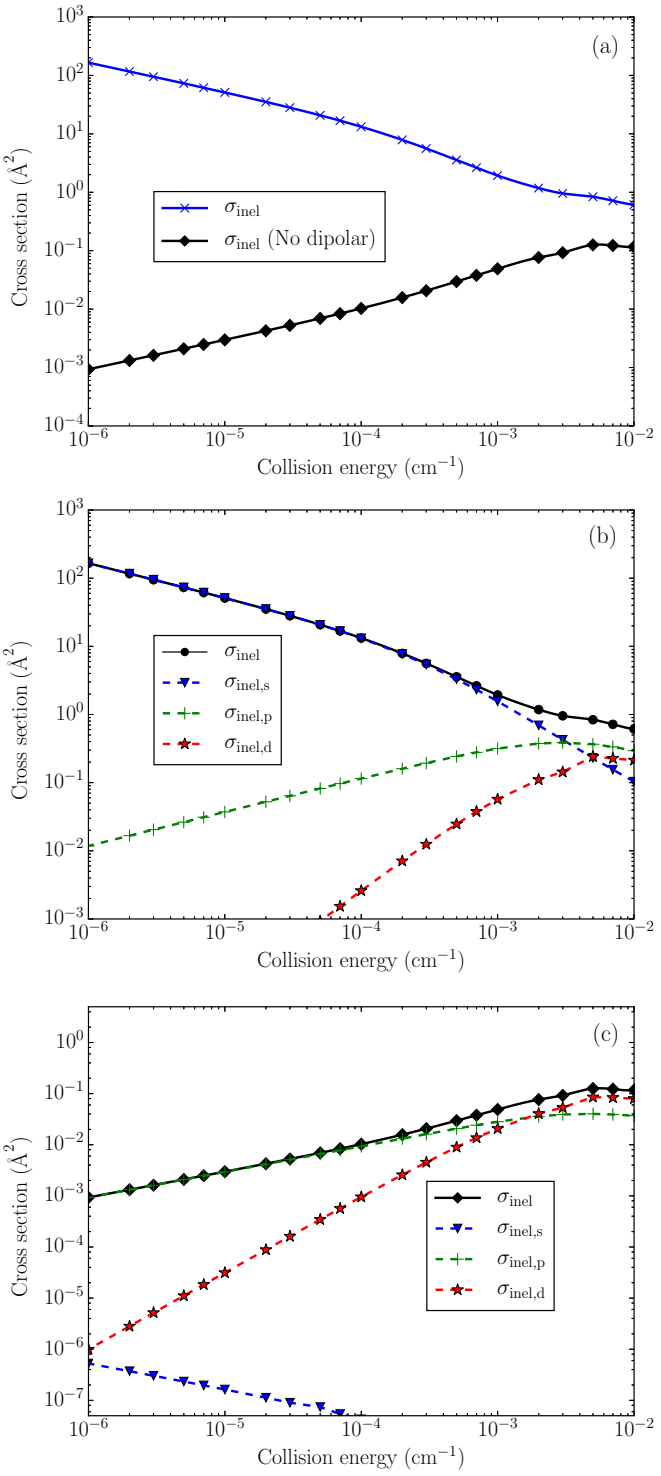

FIG. 6. (a) Collision energy dependence of the inelastic cross section calculated with (crosses) and without (diamonds) the magnetic dipole-dipole interaction for the magnetic field of 100 G. (b) Incoming partial wave decomposition of the inelastic cross section. (c) Same as in (b) but calculated without the magnetic dipole-dipole interaction.

factor of 10. This suppression compensates for the larger number of contributing terms for Li + SrOH, providing a qualitative explanation for the comparable efficiency of indirect spin-relaxation mechanisms in collisions of light and heavy molecular radicals.

Figures 3(a) and 5 show that the inelastic cross section decreases dramatically as the magnetic field is reduced below 100 G in the ultracold s-wave regime. The suppression of indirect spin relaxation is a consequence of conservation of parity and the total-angular-momentum projection M [72], which dictate that inelastic spin relaxation of the incoming s-wave channel must be accompanied by a change of the orbital angular momentum from $l = 0$ to $l = 2$. If the energy difference between the initial and final channels is small enough due to the small Zeeman splitting in a weak magnetic field, the height of the d-wave centrifugal barrier in the final channel can be larger than the initial kinetic energy in the incoming channel. Under such conditions, spin relaxation occurs by tunneling under the d-wave centrifugal barrier and is strongly suppressed. We note that this mechanism only applies to indirect spin relaxation induced by the intramolecular spin-rotation interaction.

Figures 6(b) and 6(c) compare the incoming partial wave contributions to the inelastic cross sections calculated with and without the magnetic dipole-dipole interaction. For the indirect spin-relaxation mechanism, the incoming p-wave contribution tends to exceed the incoming s-wave contribution even at very low collision energies [59,72]. In contrast, the cross sections calculated with the magnetic dipole-dipole interaction included display a more conventional partial wave structure, with the incoming s-wave contributions being dominant below $E_C = 1\times10^{-3}\,\mathrm{cm}^{-1}$ and all incoming partial wave components becoming comparable at higher collision energies. This explains the diminishing role of the indirect spin relaxation mechanism with decreasing collision energy evident in Fig. 6(a).

C. Quantum capture rates

Figure 7 shows the Li + SrOH capture rate constant as a function of temperature, with quantum and classical results shown by lines and symbols, respectively. At $T \to 0$, the quantum rate obeys the Wigner threshold law for s-wave scattering. The crossover to the multiple partial wave regime, which occurs at ca. 100 μK, manifests itself as a shallow minimum in the temperature dependence of the total capture rate. The total classical capture rate exhibits the expected divergence as $T \to 0$ due to the lack of quantum reflection in the barrierless s-wave scattering channel. On the other hand, neglecting tunneling leads to a faster decline of the contributions from higher partial waves as the temperature decreases. A combination of these two effects makes the classical capture approximation quite reasonable down to temperatures as low as 300 μK. Overall, the magnitude of the Li + SrOH capture rate and its temperature dependence are very similar to those calculated previously for the Li + CaH $\to$ LiH + Ca chemical reaction [64]. However, the larger reduced mass of the Li-SrOH collision complex and its stronger long-range dispersion forces make the crossover effect more pronounced and the classical approach more reliable for the $J > 0$ partial waves.

We note that our calculated capture rates cannot be directly compared to those obtained from quantum scattering calculations using the standard boundary conditions. However,

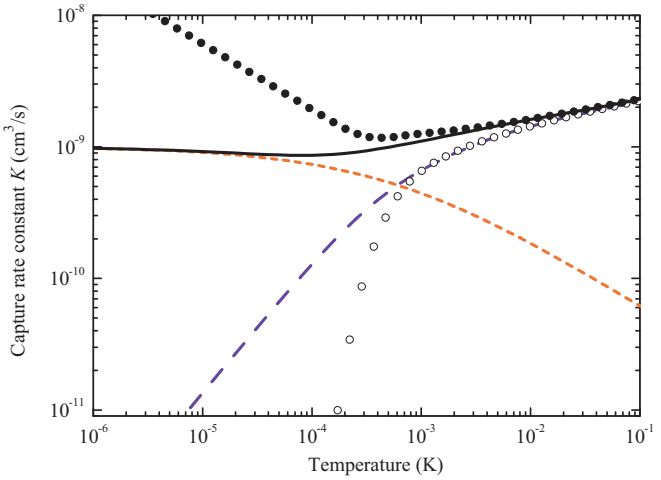

FIG. 7. Adiabatic capture rate constant for the Li + SrOH chemical reaction calculated as a function of collision energy in the absence of an external magnetic field. Quantum calculations: total rate constant (solid black line), s-wave rate constant (dotted red line), and the higher partial wave contribution (dashed blue line). Classical calculations: total rate constant (dots) and the $J > 0$ contribution (open circles).

the large magnitude of the capture rates indicates that the Li + SrOH → LiOH + Sr chemical reaction should be the dominant loss channel for the reactants colliding in non-fully-spin-polarized initial states. Assuming that the long-range behavior of the singlet and triplet PESs is identical, we obtain an upper bound to the reaction rate as 3×10^{-10} cm^3/s, one-third of the value shown in Fig. 7, and three to four orders of magnitude larger than the spin-relaxation rate for fully spin-polarized Li + SrOH collisions shown in Fig. 3. Thus, spin polarization of the reactants can be used to suppress inelastic and reactive losses in cold Li + SrOH collisions.

IV. SUMMARY AND OUTLOOK

We have studied the collisional properties of ultracold spin-polarized mixtures of SrOH molecules with Li atoms using reduced-dimensional quantum scattering calculations and a highly anisotropic triplet PES of the Li-SrOH collision complex. We present the elastic and inelastic collision cross sections over a wide range of collision energies (1×10^{-6} to 1 K) and magnetic fields (1–1000 G) along with the quantum and classical capture rates, which give an upper limit to the total Li+SrOH reaction rate. We find that inelastic spin relaxation in fully spin-polarized Li + SrOH collisions is strongly suppressed (with the ratio of elastic to inelastic collision rates $\gamma > 10^2-10^3$), suggesting good prospects for sympathetic cooling of spin-polarized SrOH molecules with Li atoms in a magnetic trap. In the context of rapid experimental progress in cooling and trapping of polyatomic radicals [20,32,35,36], our results open up the possibility of sympathetic cooling of polyatomic molecules with magnetically co-trapped ultracold alkali-metal atoms, potentially leading to new advances in low-temperature chemical dynamics and spectroscopy of large molecules in the gas phase [30,32,37].

In future work, we intend to explore the sensitivity of scattering observables to small uncertainties of the Li-SrOH interaction PES (preliminary calculations indicate that the main conclusions of this work are robust against the uncertainties). It would also be interesting to study the effect of the SrOH vibrational modes and singlet-triplet interactions neglected here [40] on cold collisions of SrOH molecules with alkali-metal atoms in arbitrary initial quantum states. Such interactions could be particularly important for heavier coolant atoms, such as K and Rb, whose use in sympathetic cooling experiments may be preferable for experimental reasons.

ACKNOWLEDGMENT

We are grateful to J. Doyle and I. Kozyryev for stimulating discussions. This work was supported by NSF Grant No. PHY-1607610.

APPENDIX: BASIS SET CONVERGENCE OF SCATTERING OBSERVABLES

Here, we explore the convergence of Li + SrOH scattering cross sections with respect to the truncation parameters $N_{\max}$ and $J_{\max}$. First, we check the convergence with respect to the maximum rotational state included in the basis set $N_{\max}$. As pointed out in Sec. II B, the small rotational constant of SrOH along with the large well depth and strong anisotropy of the Li-SrOH interaction lead to a large value of $N_{\max}$ required for convergence. Figure 8 shows the cross sections as a function of $N_{\max}$ at the collision energy of 1.0×10^{-6} cm^{-1} and the magnetic field of 100 G with $J_{\max} = 1$. We observe rapid oscillations in the calculated cross sections until $N_{\max} \sim 95$. Even after the oscillations cease at $N_{\max} > 100$, monotonous but non-negligible change of the cross sections continues until $N_{\max} = 105$. We note that there seems to be no correlation between the behavior of the elastic and inelastic cross sections as a function of $N_{\max}$ in the region of strong oscillations ($60 < N_{\max} < 95$). The convergence patterns observed at higher collision energies (e.g., 1×10^{-3} cm^{-1}) resemble

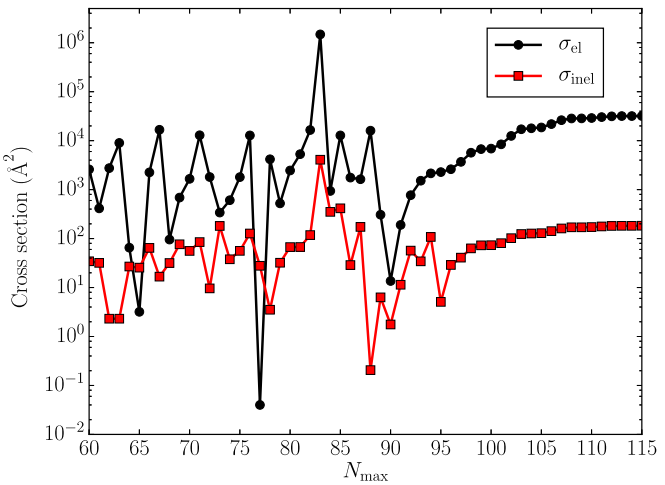

FIG. 8. Convergence of the elastic and inelastic cross sections for spin-polarized Li + SrOH collisions with respect to the number of rotational states included in the basis set at the collision energy of 1.0×10^{-6} cm^{-1}. The magnetic field is 100 G and $J_{\max} = 1$.

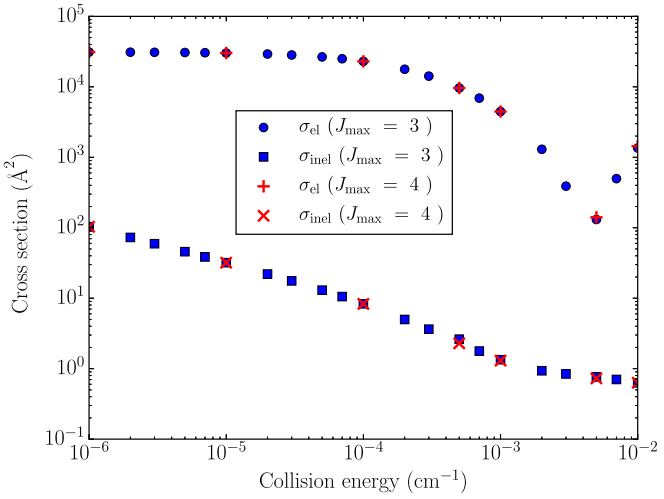

FIG. 9. Convergence of the elastic and inelastic cross sections for spin-polarized Li + SrOH collisions with respect to the number of total angular momenta included in the basis set: $J_{max} = 3$ (circles and squares) and $J_{max} = 4$ (pluses and crosses). The magnetic field is 1000 G.

those shown in Fig. 8, with the oscillations becoming less pronounced. We find that using $N_{max} = 115$ gives both the elastic and inelastic cross sections converged to within 2%.

To test the convergence of scattering observables with respect to the maximum value of the total angular momentum in the basis set J_{max}, we plot in Fig. 9 the elastic and inelastic cross sections as a function of collision energy calculated for $J_{max} = 3$ and 4. Note that since the couplings between the adjacent J blocks become stronger with increasing the B field [38], using $B = 1000$ G provides a more stringent convergence test than using $B = 100$ G. As the computational cost of the $J_{max} = 4$ calculations is very large, we limit the calculations to seven representative collision energies spanning the range 1×10^{-6} to 1×10^{-2} K. Figure 9 shows that adequate convergence of the inelastic cross sections is achieved with $J_{max} = 3$ at all collision energies. The observed convergence for $J_{max} = 3$ implies the smallness of the incoming f-wave contributions to the inelastic cross sections (described by adding the $J = 4$ block in the basis set). It also implies that the couplings between the incoming f-wave and p-wave scattering states in the entrance and exit collision channels are not critically important.

[1] L. D. Carr, D. DeMille, R. V. Krems, and J. Ye, Cold and ultracold molecules: Science, technology and applications, New J. Phys. **11**, 055049 (2009).

[2] G. Quéméner and P. S. Julienne, Ultracold molecules under control! Chem. Rev. **112**, 4949 (2012).

[3] I. Bloch, J. Dalibard, and S. Nascimbéne, Quantum simulations with ultracold quantum gases, Nat. Phys. **8**, 267 (2012).

[4] R. V. Krems, Cold controlled chemistry, Phys. Chem. Chem. Phys. **10**, 4079 (2008).

[5] B. K. Stuhl, M. T. Hummon, and J. Ye, Cold state-selected molecular collisions and reactions, Annu. Rev. Phys. Chem. **65**, 501 (2014).

[6] H. L. Bethlem, M. Kajita, B. Sartakov, G. Meijer, and W. Ubachs, Prospects for precision measurements on ammonia molecules in a fountain, Eur. Phys. J. Spec. Top. **163**, 55 (2008).

[7] E. R. Hudson, H. J. Lewandowski, B. C. Sawyer, and J. Ye, Cold Molecule Spectroscopy for Constraining the Evolution of the Fine Structure Constant, Phys. Rev. Lett. **96**, 143004 (2006).

[8] M. G. Kozlov and A. Derevianko, Proposal for a Sensitive Search for the Electric Dipole Moment of the Electron with Matrix-Isolated Radicals, Phys. Rev. Lett. **97**, 063001 (2006).

[9] J. Baron, W. C. Campbell, D. DeMille, J. M. Doyle, G. Gabrielse, Y. V. Gurevich, P. W. Hess, N. R. Hutzler, E. Kirilov, I. Kozyryev, B. R. O'Leary, C. D. Panda, M. F. Parsons, E. S. Petrik, B. Spaun, A. C. Vutha, and A. D. West (ACME Collaboration), Order of magnitude smaller limit on the electric dipole moment of the electron, Science **343**, 269 (2014).

[10] A. André, D. DeMille, J. M. Doyle, M. D. Lukin, S. E. Maxwell, P. Rabl, R. J. Schoelkopf, and P. Zoller, A coherent all-electrical interface between polar molecules and mesoscopic superconducting resonators, Nat. Phys. **2**, 636 (2006).

[11] K.-K. Ni, S. Ospelkaus, M. H. G. de Miranda, A. Pe'er, B. Neyenhuis, J. J. Zirbel, S. Kotochigova, P. S. Julienne, D. S. Jin, and J. Ye, A high phase-space-density gas of polar molecules, Science **322**, 231 (2008).

[12] S. Ospelkaus, K.-K. Ni, D. Wang, M. H. G. de Miranda, B. Neyenhuis, G. Quéméner, P. S. Julienne, J. L. Bohn, D. S. Jin, and J. Ye, Quantum-state controlled chemical reactions of ultracold KRb molecules, Science **327**, 853 (2010).

[13] J. W. Park, S. A. Will, and M. W. Zwierlein, Ultracold Dipolar Gas of Fermionic ^{23}Na^{40}K Molecules in Their Absolute Ground State, Phys. Rev. Lett. **114**, 205302 (2015).

[14] E. S. Shuman, J. F. Barry, and D. DeMille, Laser cooling of a diatomic molecule, Nature (London) **467**, 820 (2010).

[15] J. F. Barry, D. J. McCarron, E. B. Norrgard, M. H. Steinecker, and D. DeMille, Magneto-optical trapping of a diatomic molecule, Nature (London) **512**, 286 (2014).

[16] E. B. Norrgard, D. J. McCarron, M. H. Steinecker, M. R. Tarbutt, and D. DeMille, Submillikelvin Dipolar Molecules in a Radio-Frequency Magneto-Optical Trap, Phys. Rev. Lett. **116**, 063004 (2016).

[17] M. T. Hummon, M. Yeo, B. K. Stuhl, A. L. Collopy, Y. Xia, and J. Ye, 2D Magneto-Optical Trapping of Diatomic Molecules, Phys. Rev. Lett. **110**, 143001 (2013).

[18] A. L. Collopy, M. T. Hummon, M. Yeo, B. Yan, and J. Ye, Prospects for a narrow line MOT in YO, New J. Phys. **17**, 055008 (2015).

[19] Hsin-I Lu, I. Kozyryev, B. Hemmerling, J. Piskorski, and J. M. Doyle, Magnetic Trapping of Molecules via Optical Loading and Magnetic Slowing, Phys. Rev. Lett. **112**, 113006 (2014).

[20] I. Kozyryev, L. Baum, K. Matsuda, B. L. Augenbraun, L. Anderegg, A. P. Sedlack, and J. M. Doyle, Sisyphus Laser Cooling of a Polyatomic Molecule, Phys. Rev. Lett. **118**, 173201 (2017).

[21] M. Zeppenfeld, B. G. U. Englert, R. Glöckner, A. Prehn, M. Mielenz, C. Sommer, L. D. van Buuren, M. Motsch, and G. Rempe, Sisyphus cooling of electrically trapped polyatomic molecules, Nature (London) **491**, 570 (2012).

[22] A. Prehn, M. Ibrügger, R. Glöckner, G. Rempe, and M. Zeppenfeld, Optoelectrical Cooling of Polar Molecules to Submillikelvin Temperatures, Phys. Rev. Lett. **116**, 063005 (2016).

[23] M. Lara, J. L. Bohn, D. Potter, P. Soldan, and J. M. Hutson, Ultracold Rb-OH Collisions and Prospects for Sympathetic Cooling, Phys. Rev. Lett. **97**, 183201 (2006).

[24] M. L. González-Martínez and J. M. Hutson, Ultracold Hydrogen Atoms: A Versatile Coolant to Produce Ultracold Molecules, Phys. Rev. Lett. **111**, 203004 (2013).

[25] M. T. Hummon, T. V. Tscherbul, J. Kłos, H.-I Lu, E. Tsikata, W. C. Campbell, A. Dalgarno, and J. M. Doyle, Cold N+NH Collisions in a Magnetic Trap, Phys. Rev. Lett. **106**, 053201 (2011).

[26] P. Żuchowski and J. M. Hutson, Cold collisions of N atoms and NH molecules in magnetic fields, Phys. Chem. Chem. Phys. **13**, 3669 (2011).

[27] W. Skomorowski, M. L. González-Martínez, R. Moszynski, and J. M. Hutson, Cold collisions of an open-shell S-state atom with a $^2\Pi$ molecule: N(^{4}S) colliding with OH in a magnetic field, Phys. Chem. Chem. Phys. **13**, 19077 (2011).

[28] A. O. G. Wallis and J. M. Hutson, Production of Ultracold NH Molecules by Sympathetic Cooling with Mg, Phys. Rev. Lett. **103**, 183201 (2009).

[29] T. V. Tscherbul, J. Kłos, and A. A. Buchachenko, Ultracold spin-polarized mixtures of $^2\Sigma$ molecules with *S*-state atoms: Collisional stability and implications for sympathetic cooling, Phys. Rev. A **84**, 040701(R) (2011).

[30] T. V. Tscherbul, H.-G. Yu, and A. Dalgarno, Sympathetic Cooling of Polyatomic Molecules with *S*-State Atoms in a Magnetic Trap, Phys. Rev. Lett. **106**, 073201 (2011).

[31] T. V. Tscherbul, T. A. Grinev, H.-G. Yu, A. Dalgarno, J. Kłos, L. Ma, and M. H. Alexander, Cold collisions of polyatomic molecular radicals with *S*-state atoms in a magnetic field: An *ab initio* study of He + $CH_2(\tilde{X})$ collisions, J. Chem. Phys. **137**, 104302 (2012).

[32] Y. Liu, M. Vashishta, P. Djuricanin, S. Zhou, W. Zhong, T. Mittertreiner, D. Carty, and T. Momose, Magnetic Trapping of Cold Methyl Radicals, Phys. Rev. Lett. **118**, 093201 (2017).

[33] Yu. V. Suleimanov, T. V. Tscherbul, and R. V. Krems, Efficient method for quantum calculations of molecule-molecule scattering properties in a magnetic field, J. Chem. Phys. **137**, 024103 (2012).

[34] Yu. V. Suleimanov and T. V. Tscherbul, Cold NH-NH collisions in a magnetic field: Basis set convergence vs sensitivity to the interaction potential, J. Phys. B **49**, 204002 (2016).

[35] I. Kozyryev, L. Baum, K. Matsuda, P. Olson, B. Hemmerling, and J. M. Doyle, Collisional relaxation of vibrational states of SrOH with He at 2 K, New J. Phys. **17**, 045003 (2015).

[36] I. Kozyryev, L. Baum, K. Matsuda, B. Hemmerling, and J. M. Doyle, Radiation pressure force from optical cycling on a polyatomic molecule, J. Phys. B **49**, 134002 (2016).

[37] I. Kozyryev, L. Baum, K. Matsuda, and J. M. Doyle, Proposal for laser cooling of complex polyatomic molecules, Chem. Phys. Chem. **17**, 3641 (2016).

[38] T. V. Tscherbul and A. Dalgarno, Quantum theory of molecular collisions in a magnetic field: Efficient calculations based on the total angular momentum representation, J. Chem. Phys. **133**, 184104 (2010).

[39] M. A. Anderson, W. L. Barclay, Jr., and L. M. Ziurys, The millimeter-wave spectrum of the SrOH and SrOD radicals, Chem. Phys. Lett. **196**, 166 (1992).

[40] M. Warehime and J. Kłos, Nonadiabatic collisions of CaH with Li: Importance of spin-orbit-induced spin relaxation in spin-polarized sympathetic cooling of CaH, Phys. Rev. A **92**, 032703 (2015).

[41] P. J. Knowles, C. Hampel, and H.-J. Werner, Coupled cluster theory for high spin, open shell reference wave functions, J. Chem. Phys. **99**, 5219 (1993) [Erratum: **112**, 3106(E) (2000)].

[42] H.-J. Werner and P. J. Knowles, A second order multiconfiguration SCF procedure with optimum convergence, J. Chem. Phys. **82**, 5053 (1985).

[43] P. J. Knowles and H.-J. Werner, An efficient second-order MC SCF method for long configuration expansions, Chem. Phys. Lett. **115**, 259 (1985).

[44] H. Li, H. Feng, W. Sun, Y. Zhang, Q. Fan, K. A. Peterson, Y. Xie, and H. F. Schaefer III, The alkaline earth dimer cations (Be^{2+}, Mg^{2+}, Ca^{2+}, Sr^{2+}, and Ba^{2+}). Coupled cluster and full configuration interaction studies, Mol. Phys. **111**, 2292 (2013).

[45] I. S. Lim, H. Stoll, and P. Schwerdtfeger, Relativistic small-core energy-consistent pseudopotentials for the alkaline-earth elements from Ca to Ra, J. Chem. Phys. **124**, 034107 (2006).

[46] T. H. Dunning, Jr., Gaussian basis sets for use in correlated molecular calculations. I. The atoms boron through neon and hydrogen, J. Chem. Phys. **90**, 1007 (1989).

[47] R. Prosmiti, C. Cunha, P. Villarreal, and G. Delgado-Barrio, The van der Waals potential energy surfaces and structures of He-ICl and Ne-ICl clusters, J. Chem. Phys. **117**, 7017 (2002).

[48] A. Gertych and J. Koput, *Ab initio* prediction of the structure and vibration-rotation spectroscopic properties of Na_2OH and K_2OH, J. Comput. Chem. **31**, 1542 (2010).

[49] T. V. Tscherbul and R. V. Krems, Controlling Electronic Spin Relaxation of Cold Molecules with Electric Fields, Phys. Rev. Lett. **97**, 083201 (2006).

[50] E. Abrahamsson, T. V. Tscherbul, and R. V. Krems, Inelastic collisions of cold polar molecules in nonparallel electric and magnetic fields, J. Chem. Phys. **127**, 044302 (2007).

[51] NIST-JANAF Thermochemical Tables, version 1.0, NIST, Gaithersburg, MD, 1985, http://kinetics.nist.gov/janaf/

[52] A. Kramida, Yu. Ralchenko, J. Reader, and NIST ASD Team. NIST Atomic Spectra Database, version 5.4, NIST, Gaithersburg, MD, 2016, http://physics.nist.gov/asd

[53] S. F. Boys and F. Bernardi, The calculation of small molecular interactions by the differences of separate total energies. Some procedures with reduced errors, Mol. Phys. **19**, 553 (1970).

[54] H.-J. Werner, P. J. Knowles, G. Knizia, F. R. Manby, and M. Schütz, Molpro: A general-purpose quantum chemistry program package, WIREs Comput. Mol. Sci. **2**, 242 (2012).

[55] MOLPRO, version 2012.1, a package of *ab initio* programs, H.-J. Werner, P. J. Knowles, G. Knizia, F. R. Manby, M. Schütz, and others; see http://www.molpro.net

[56] T. S. Ho and H. Rabitz, A general method for constructing multidimensional molecular potential energy surfaces from *ab initio* calculations, J. Chem. Phys. **104**, 2584 (1996).

[57] T. Hollebeek, T. S. Ho, and H. Rabitz, Constructing multidimensional molecular potential energy surfaces from *ab initio* data, Annu. Rev. Phys. Chem. **50**, 537 (1999).

[58] See Supplemental Material at http://link.aps.org/supplemental/10.1103/PhysRevA.95.063421 for a FORTRAN code for the Li-SrOH PES.

[59] R. V. Krems and A. Dalgarno, Quantum-mechanical theory of atom-molecule and molecular collisions in a magnetic field: Spin depolarization, J. Chem. Phys. **120**, 2296 (2004).

[60] D. E. Manolopoulos, An improved log derivative method for inelastic scattering, J. Chem. Phys. **85**, 6425 (1986).

[61] M. H. Alexander and D. E. Manolopoulos, A stable linear reference potential algorithm for solution of the quantum close-coupled equations in molecular scattering theory, J. Chem. Phys. **86**, 2044 (1987).

[62] L. M. C. Janssen, A. van der Avoird, and G. C. Groenenboom, On the role of the magnetic dipolar interaction in cold and ultracold collisions: Numerical and analytical results for $NH(^3\Sigma) + NH(^3\Sigma)$, Eur. Phys. J. D **65**, 177 (2011).

[63] A. A. Buchachenko, Numerical method of quantum capture probability determination for molecular collisions at ultralow temperatures, Moscow Univ. Chem. Bull. **67**, 159 (2012).

[64] T. V. Tscherbul and A. A. Buchachenko, Adiabatic channel capture theory applied to cold atom-molecule reactions: Li + CaH $\rightarrow$ LiH + Ca at 1 K, New J. Phys. **17**, 035010 (2015).

[65] D. G. Truhlar and A. Kuppermann, Exact tunneling calculations, J. Am. Chem. Soc. **93**, 1840 (1971).

[66] J. M. Hutson, M. Beyene, and M. L. González-Martínez, Dramatic Reductions in Inelastic Cross Sections for Ultracold Collisions near Feshbach Resonances, Phys. Rev. Lett. **103**, 163201 (2009).

[67] J. P. Burke, Jr., J. L. Bohn, B. D. Esry, and C. H. Greene, Prospects for Mixed-Isotope Bose-Einstein Condensates in Rubidium, Phys. Rev. Lett. **80**, 2097 (1998).

[68] J. P. Burke, Theoretical investigation of cold alkali atom collisions, Ph.D. thesis, University of Colorado, 1999.

[69] T. V. Tscherbul, Y. V. Suleimanov, V. Aquilanti, and R. V. Krems, Magnetic field modification of ultracold molecule-molecule collisions, New J. Phys. **11**, 055021 (2009).

[70] J. Pérez-Ríos, J. Campos-Martínez, and M. I. Hernández, Ultracold $O_2 + O_2$ collisions in a magnetic field: On the role of the potential energy surface, J. Chem. Phys. **134**, 124310 (2011).

[71] R. V. Krems, A. Dalgarno, N. Balakrishnan, and G. C. Groenenboom, Spin-flipping transitions in $^2\Sigma$ molecules induced by collisions with structureless atoms, Phys. Rev. A **67**, 060703(R) (2003).

[72] A. Volpi and J. L. Bohn, Magnetic-field effects in ultracold molecular collisions, Phys. Rev. A **65**, 052712 (2002).